Article

Optical Properties of RF-Magnetron-Sputtered Polycrystalline Cu_3N Thin Films Determined by UV/visible/NIR Spectroscopic Ellipsometry: Eco-Friendly Light Absorber

Emilio Márquez [1,*], Eduardo Blanco[1], Marcos García-Gurrea[1], Manuel Cintado Puerta[1], Manuel Domínguez de la Vega[1], Manuel Ballester[2], Jose M. Mánuel[1] , Maribel A. Rodríguez-Tapiador[3], Susana M. Fernández[3]

[1] Department of Condensed-Matter Physics, Faculty of Science, University of Cadiz, 11510 Puerto Real, Spain
[2] Department of Computer Sciences, Northwestern University, 633 Clark St, Evanston, IL 60208, USA
[3] Environmental and Energetic Devices Unit, Energy Department, CIEMAT, Avenida Complutense 40, 28040 Madrid, Spain
* Correspondence: emilio.marquez@uca.es

Abstract: Copper nitride (Cu_3N), a *metastable* semiconductor material, but with reasonably-high-stability at room temperature, is drawing a great deal of attention as a very promising next-generation, earth-abundant, thin-film solar absorber. Its non-toxicity, on the other hand, makes it a very attractive *eco-friendly* semiconducting material. In the present work, Cu_3N thin films were grown by employing radio-frequency magnetron sputtering, at room temperature, with 50-W RF-power, and partial nitrogen pressures of 8.0 and 1.0, onto glass substrates. Thus, the influence of argon on the optical properties of the Cu_3N thin films was studied, with the goal of being able to achieve a low-cost, light absorber material, with appropriate properties in order to substitute the more conventional silicon, in photovoltaic cells. Variable-angle spectroscopic ellipsometry measurements have been conducted at three angles, 50°, 60°, and 70°, respectively, in order to obtain the two ellipsometric parameters psi, ψ, and delta, Δ, respectively. For the constructed optical model, the bulk planar Cu_3N layer is described by a one-dimensional *graded-index* model, combine with the mixture of a Tauc-Lorentz oscillator and up to four Gaussian oscillators, whereas a BEMA model with 50 %-air-void is adopted in order to account for the existing surface-roughness layer. In addition, the optical properties such as the energy-band gap, and refractive index and absorption coefficient, were determined in order to assess the actual capability of this material as a light absorber for solar cells. The direct and indirect band gap energies were accurately calculated, and they were found to be in the ranges of 2.14-2.21 eV and very clse to 1.50 eV, respectively.

Keywords: copper-nitride semiconductor; RF-magnetron sputtering; spectroscopic ellipsometry

Citation: Emilio Márquez, Eduardo Blanco, Marcos García-Gurrea, Manuel Cintado, Manuel Domínguez de la Vega, Jose M. Mánuel, Manuel Ballester, Maribel A. Rodríguez-Tapiador, Susana M. Fernández Optical Properties of RF-magnetron-sputtered polycrystalline Cu_3N thin films determined by UV/visible/NIR spectroscopic ellipsometry: eco-friendly light absorber. *Preprints* **2022**, *1*, 0. https://doi.org/

1. Introduction

Transition-metal nitride thin-film materials, such as copper nitride (Cu_3N), exhibit very attractive and remarkable physical properties, such as optical, electrical and energy-storage properties, which have enable to this particular material to be employed in many technological-application fields [1,2]. Consequently, copper nitride has drawn great deal of attention as a new *eco-friendly* solar-absorber material, for flexible and lightweight thin-film photovoltaic cells [3,4]. This metastable semiconductor material is *non-toxic*, made up of earth-abundant elements, and its band-gap energy can be relatively easily tunable, depending upon both the manufacturing conditions, and the deposition techniques. Among the fields of applications, it can be indicated the following: integrated circuits, photo-detectors, optoelectronics, and energy-conversion applications [5–7]. Emphasizing again the mentioned specific use of Cu_3N as a novel *solar* absorber thin-layer material for photovoltaic-cell technology [8]: Its development has caused a notable interest with the goal of being introduced into novel designs, within a future generation of cost-effective solar cells. This recently-gained attention as a *light* absorber in solar-cell, is mainly based upon its mentioned clear non-toxicity and significant earth abundance, which produces such an environmentally friendly material. Furthermore, the theoretically-predicted band-gap value for Cu_3N is approximately 0.9 eV [9,10], but its experimentally-obtained values of the indirect and direct band gaps are found to be within the energy ranges from 1.17 eV up to 1.69 eV, and from 1.72 eV up to 2.38 eV, respectively [10,11]. These obtained values imply that the Cu_3N semiconductor can be considered a promising

 doi:10.20944/preprints202305.1426.v1

candidate as a next-generation light absorber, that is, a realistic candidate in order to fully substitute the more conventional silicon in PV industry.

Such a large reported differences found in the band gap can be explained as a possible difference in the stoichiometry of the Cu-N binary system, and also due to the existence of oxygen impurities into the crystal lattice. This material, on the other hand, possesses interestingly an extremely high absorption coefficient larger than 10^5 cm^{-1} above approximately 2.0 eV [12], as will be accurately found in this work, which underlines once more the above-mentioned potential role as an solar-light absorber for photovoltaic-cell technologies.

In the present investigation, the complex index of refraction of the Cu_3N thin films is determined via variable-angle spectroscopic ellipsometry (VASE) measurements [13], which were conducted at three different angles of incidence, 50°, 60°, and 70°, respectively, to obtain the two ellipsometric parameters psi, ψ, and delta, Δ, respectively. In order to achieve an excellent fit with the measured values of ψ and Δ, it is of paramount importance to construct a valid optical model. In our particular case, a one-dimensional *graded-index* model throughout the whole layer, from the bottom to the top, combined with a mixture of one Tauc-Lorentz (TL) oscillator [14–18], and up to four Gaussian (Gau) oscillators, are successfully adopted to account for the *bulk* copper-nitride layer, whereas a Bruggeman-effective-medium approximation (BEMA) model [19], with 50 %-air-void, is selected in order to describe the existing surface-roughness layer. As a result, the optical constants of the Cu_3N thin films are accurately determined in the measured wavelength range of 300 to 2200 nm. Our constructed optical model for extracting the optical constants of Cu_3N thin layers is similar to the optical model suggested by Yan *et al.* [20–22], for the particular case of cesium-lead-bromide ($CsPbBr_3$) thin films, where they also adopted a similar combination of several TL and Gau oscillators, and the front-rough-superficial layer was included in the model, as well.

Finally, it must be pointed out that there is generally very inconsistent and ambiguous information about the optical properties of copper-nitride thin films, which is most likely to be caused by the existing differences in the particular synthesis technology employed in each case. Hence, it is particularly relevant and clarifying the present spectro-ellipsometric study of the refractive index, n, extinction coefficient, k, and absorption coefficient, α, in the UV/visible/NIR spectral range, carried out in this work.

2. Experimental procedure: materials and methods

The growth of the Cu_3N thin films was performed by employing a commercial MVSystem LLC (Golden, CO, USA), single-chamber sputtering system, where the gun was radio-frequency (RF) operated, and it was vertically movable. The transparent substrates employed were Corning glass 1737F (Corning Inc, USA). The 3-in diameter and 6-mm-thick target was manufactured by Lesker Company (St. Leonards-on-Sea, UK), and it had a 99.99 % purity. The glass substrate, on the other hand, was cleaned by an ultrasonic bath with ethanol and deionized water during 10 min, and it was lastly immersed in isopropyl alcohol; next, all the used glass substrates were carefully dried by blowing nitrogen on them. The RF-sputtering-process chamber was pumped down to a base pressure of 10^{-5} Pa, and the deposition process was performed in an environment with the total working gas pressure set to 5.0 Pa, and it was controlled by using a butterfly-type valve. The target-to-substrate distance was always set to a conveniently selected nearly 10 cm. The RF power was set to 50 W, and the corresponding grown time was 60 and 90 min. All the thin-film depositions were carried out at *room temperature*. The complete set of growth conditions of our specimens are listed in Table 1.

The atomic structure, morphology, and chemical composition of the Cu_3N thin films were analyzed by X-ray diffraction (XRD), atomic force microscopy (AFM), and energy-dispersive X-ray spectroscopy (EDX), respectively. The *polycrystalline* structure of the Cu_3N samples were studied by the corresponding XRD diffraction patterns, measured with a PANalytical power diffractometer, model X'Pert MPD/MRD, by using CuK_α radiation ($\lambda = 1.54$ Å). The scanned 2θ-range was 10-60°, at a step size of 0.1°. The topography of the Cu_3N film surface was measured by using a

 doi:10.20944/preprints202305.1426.v1

Table 1. Deposition conditions for the growth of Cu_3N by RF-magnetron-sputtering deposition.

Growth Conditions						
Sample ID	Total pressure (Pa)	N_2 flux(sccm)	Ar flux (sccm)	Partial N_2 Pressure	RF Power (W)	Deposition time (min)
#1360	5.0	20	10	0.8	50	60
#1460	5.0	20	0	1.0	50	60
#1490	5.0	20	0	1.0	50	90

standard AFM microscope (Dimension Icon, Bruker, USA), in peakForce tapping mode, and with Bruker SeanAsyst-Air probes (radius 5 nm). The surface roughness of the thin-film samples was estimated by its root-mean-square value. Finally, the optical transmission spectra were measured at normal incidence, by using a UV/visible/NIR, double-beam, Perkin-Elmer Lambda-1050 spectrophotometer, and also with a single-beam VASE spectroscopic ellipsometer.

Cu_3N thin-layer thickness, profile texture, and surface topography of the Cu_3N material were characterized via scanning electron microscopy (SEM). As a first step, the samples were mechanically cleaved in order to obtain SEM micrographs from cross-section profiles along the growth direction, which allowed determining the average thickness of each Cu_3N layer. Afterwards, gold thin layers were deposited on all samples surfaces to avoid charging effects, due to the interaction between the electron beam and the non-conductive sample. This was achieved by using a magnetron deposition process, via plasma, in a 208HR-Cressington Sputter Coater (Cressington Scientific Instruments, UK).

The spectro-ellipsometric spectra ψ and Δ, respectively, were measured over the spectral range of 300-2200 nm with steps of 10 nm, at room temperature, by making use of a Woollam V-VASE spectroscopic ellipsometer. It is essentially a rotating analyzing ellipsometer, with a Berek computer-controlled, adjustable MgF_2-waveplate retarder (the so-called *automatic retarder*), which is used to very-accurately introduce a beam path delay, over a wide spectral range. This variable retarder allows to adjust the input polarization in order to provide a reflected beam, which is always close to circular polarization, and thus the system will measure Δ accurately over the entire angular range of 0-360°. Moreover, the *autoretarder*-ellipsometer configuration permits the measurement of the '%-depolarization', which can be correlated with thickness nonuniformities of the studied samples, enabling a better fitting of the two ellipsometric angles ψ and Δ, respectively, in these particular cases. The data analysis was systematically performed with the WVASE32 software, from J.A. Woollam [23].

3. Preliminary structural and morphological characterizations

XRD patterns of three as-deposited Cu_3N thin films are shown in Fig. 1. The main diffraction peaks identified as the $(1\,0\,0)$, $(1\,1\,1)$, and $(2\,0\,0)$ crystallographic planes, represent a *polycrystalline* Cu_3N film (card number 00-047-1088), in *cubic*, *anti*-ReO_3 structure (space group $Pm\bar{3}m$, number 221, first reported by Juza and Hahn [24]). No evidence whatsoever for Cu-phase and CuO formation was found in the present XRD diagrams.

Preprints (www.preprints.org) | NOT PEER-REVIEWED | Posted: 19 May 2023 doi:10.20944/preprints202305.1426.v1

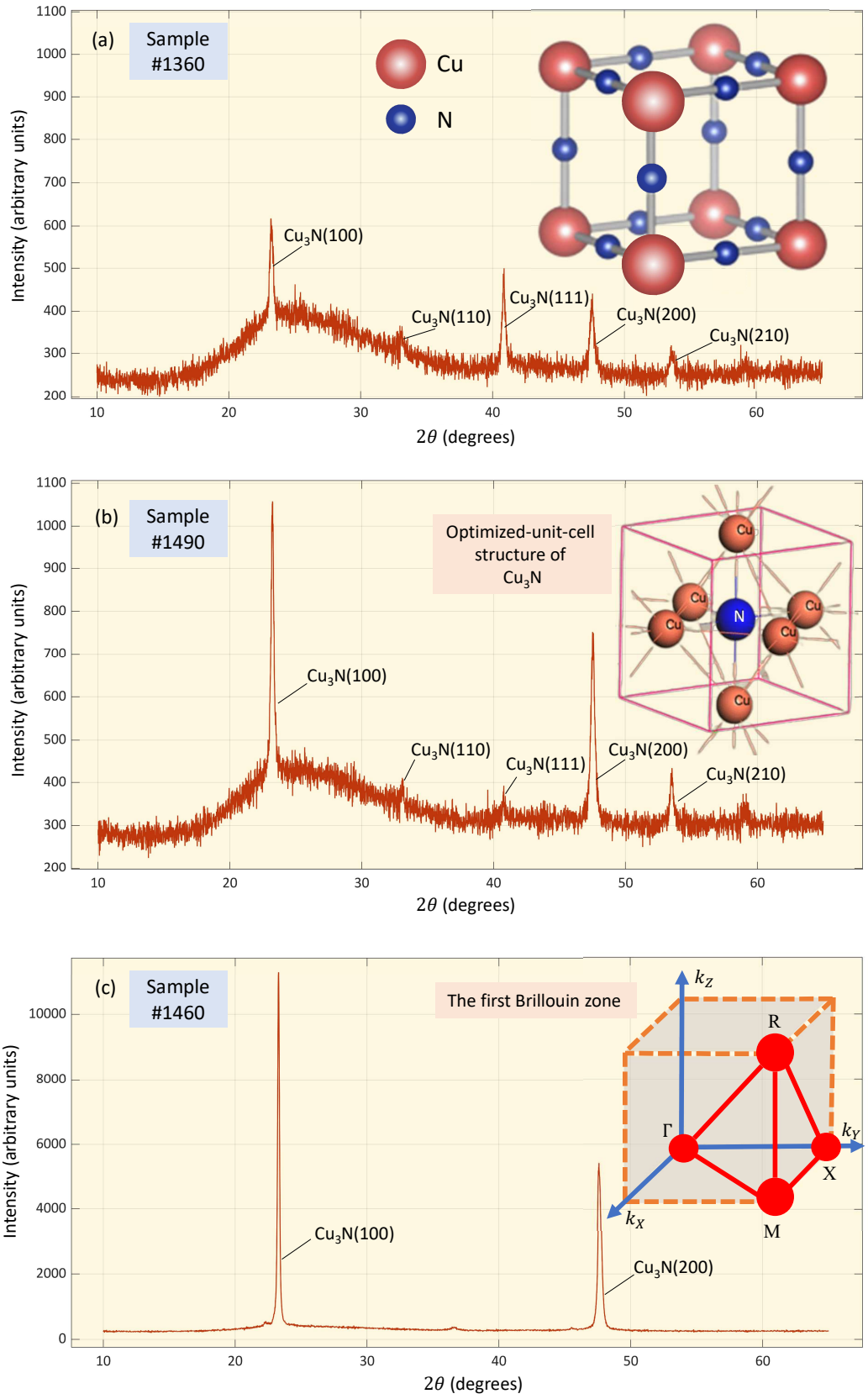

Figure 1. X-ray diffraction (XRD) patterns of the three copper nitride thin films, deposited onto glass substrates, and corresponding specifically to (a) specimen #1360, (b) specimen #1490, and (c) specimen #1460. The 3D cubic structure of Cu_3N is clearly illustrated as an inset in Fig. 1b. This cubic structure of the *unit cell* contains six Cu atoms, and their fractional coordinates are the following: $(0,0.5,0.5)$, $(0.5,0,0.5)$, and $(0.5,0.5,0)$. The fractional coordinate of the N atom is $(0.5,0.5,0.5)$, which is in the center position of the present Cu molecules[25]. *First Brillouin zone* of Cu_3N, with the high-symmetry points Γ $(0,0,0)$, M $(\frac{\pi}{a},\frac{\pi}{a},0)$, R $(\frac{\pi}{a},\frac{\pi}{a},\frac{\pi}{a})$, and X $(0,\frac{\pi}{a},0)$, labeled and joined by red lines [26], shown as an inset in Fig. 1c.

Preprints (www.preprints.org) | NOT PEER-REVIEWED | Posted: 19 May 2023 doi:10.20944/preprints202305.1426.v1

As it was previously said, the surface morphology of the Cu_3N thin-film samples was carefully analyzed by AFM microscopy. Figure 2 displays the $1.0\,\mu m \times 1.0\,\mu m$ and $2.0\,\mu m \times 2.0\,\mu m$ bi-dimensional AFM micrographs of the three Cu_3N layers, sputtered all of them at a *total* gas pressure of 5.0 Pa. Table 2 indicates the values of the three considered surface-roughness parameters, S_q, S_a, and S_z, respectively, determined with the help of the software connected with this device, and by using 2D-AFM images displayed in Fig. 2. It should be stressed that all these calculations led to an estimated uncertainty of less than around 10 %. According to the three measured surface roughness parameters, S_q, S_a, and S_z, respectively, the *as-deposited* Cu_3N thin-layer samples under study do certainly exhibit a *relatively large* surface roughness.

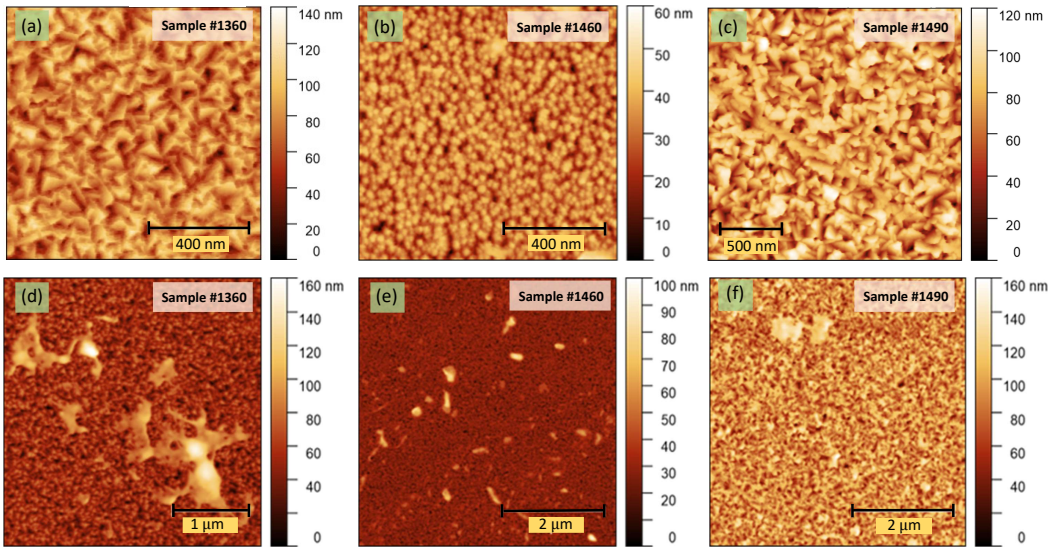

Figure 2. The two-dimensional AFM images of Cu_3N thin-filmS: (a) and (d) Sample #1360, (b) and (e) Sample #1460, (c) and (f) Sample #1490, respectively.

Table 2. Surface-roughness parameters determined from AFM $1.0\,\mu m \times 1.0\,\mu m$ and $2.0\,\mu m \times 2.0\,\mu m$ images of the copper nitride thin layer, grown by RF-magnetron sputtering on glass substrates.Values of the root-mean-square height, S_q, the arithmetical-mean height, S_a, and the maximum height, S_z, corresponding to the two representative Cu_3N thin-film samples.

Cu_3N-thin-film Sample ID	**#1360**	**#1460**	**#1490**
Figure ID	**(a)**	**(b)**	**(c)**
AFM-Scanning Area	$1.0\,\mu m \times 1.0\,\mu m$	$1.0\,\mu m \times 1.0\,\mu m$	$2.0\,\mu m \times 2.0\,\mu m$
S_q (Root-Mean-Square Height), nm	16.5	6.6	18.0
S_a (Arithmetical-Mean Height), nm	13.2	5.3	14.5
S_z (Maximum Height), nm	125	52.7	122
Cu_3N-thin-film Sample ID	**#1360**	**#1460**	**#1490**
Figure ID	**(d)**	**(e)**	**(f)**
AFM-Scanning Area	$3.3\,\mu m \times 3.3\,\mu m$	$5.0\,\mu m \times 5.0\,\mu m$	$5.0\,\mu m \times 5.0\,\mu m$
S_q (Root-Mean-Square Height), nm	19.1	7.3	19.9
S_a (Arithmetical-Mean Height), nm	14.4	5.3	16.0
S_z (Maximum Height), nm	163.6	94.1	159.5

It is reasonable therefore that the corresponding obtained values by the ellipsometric models for the BEMA surface-roughness layer, d_{rough} (see Table 3), be *larger* than those determined by the $1.0\,\mu m \times 1.0\,\mu m$ and $2.0\,\mu m \times 2.0\,\mu m$ AFM images. That is, taking into account the fact that the size of the light-spot of the spectroscopic ellipsometer is very much bigger than that of the previous AFM images, it is indeed likely to occur that d_{rough} is larger than the three parameters S_q, S_a, and S_z,

Preprints (www.preprints.org) | NOT PEER-REVIEWED | Posted: 19 May 2023 doi:10.20944/preprints202305.1426.v1

respectively.

Figure 3, on the other hand, shows cross-sectional-view SEM images of the as-grown Cu_3N thin layers, deposited in a $N_2 + Ar$ environment (Figure 3a), in the particular case of the sample #1390, and without Ar in the case of sample #1490. The SEM-measured values of the film thickness clearly confirm the excellent accuracy of the layer thickness calculated by UV/visible/NIR spectroscopic ellipsometry, as will be shown in detail below. The SEM images also corroborated that film surface were not extremely rough and nonuniform, and are mainly made up of typical *columnar* grains, typical of the present sputtering deposition technique [27]. Importantly, all the results found by the SEM microscopy are certainly consistent with those obtained from the previous AFM-microscopy analysis.

Also, in order to register SEM images revealing the Cu_3N layer texture, micrometric trenches were made transversely to the surface. This was carried out using Ga^+-ion beam, via a focused ions beam (FIB) module. SEM images were recorded by using secondary electron detectors, 5-kV accelerating voltages, and working distances ranging from 6 to 7 mm . Furthermore, the chemical composition of the Cu_3N layers were found by using an electron dispersive X-ray spectroscopy module, attached to the electron microscope. EDX spectra were obtained by using electron probes accelerated at 30-kV voltages.

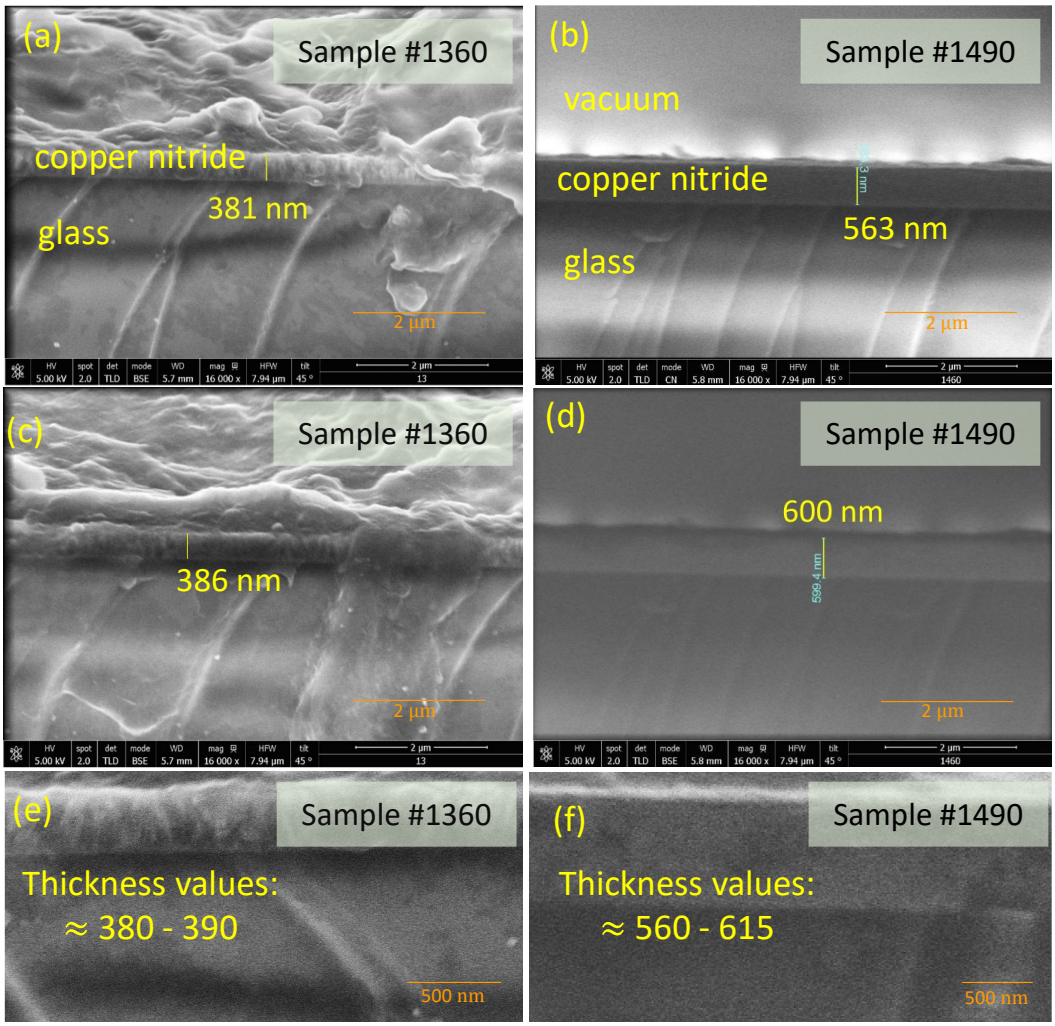

Figure 3. High-magnification cross-sectional SEM images of the studied in (a) $N_2 + Ar$, (specimen #1360), and (b) pure N_2 (specimen #1490) environments.

Preprints (www.preprints.org) | NOT PEER-REVIEWED | Posted: 19 May 2023 doi:10.20944/preprints202305.1426.v1

We performed the conventional FIB sample-preparation procedures, before undertaking the EDX analysis. In our EDX study of the present Cu_3N thin-film specimens (see the measured EDX maps displayed in Fig. 4), oxygen and nitrogen, as light elements, were *not* detected with high sensitivity, but it can be observed that the oxygen signal is, indeed, more intense near the glass-substrate region (the glass having both silica and alumina). The nitrogen signal, on the other hand, notably decreases near the Cu_3N-glass interface, and increases, on the contrary, in the *bulk* Cu_3N layer. However, it must be pointed out that an increase of oxygen content and a decrease of nitrogen content near the surface of the film is *not* seen. Significantly, from the present EDX maps (Fig. 4), it is *not* reasonable to speculate with the existence of a very-thin-copper-oxide layer, at the surface of the Cu_3N thin film.

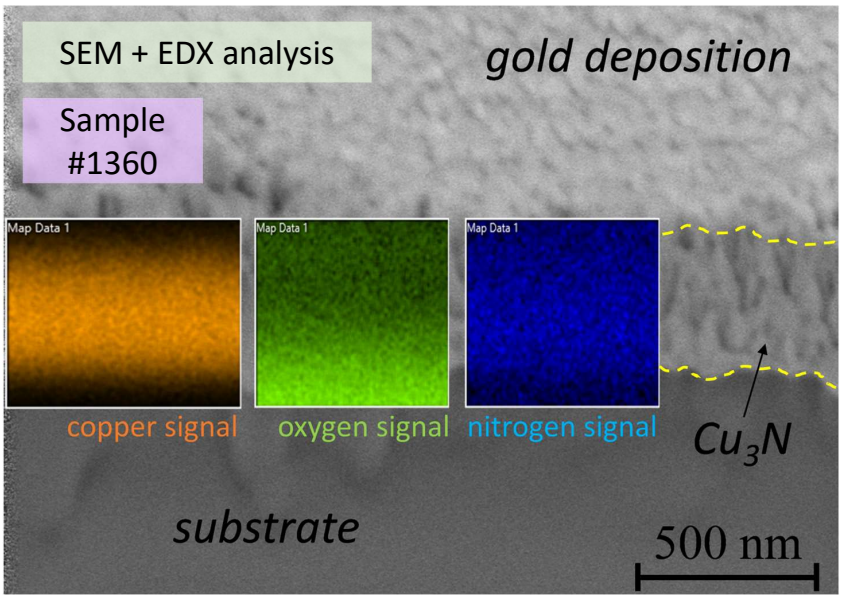

Figure 4. Cross-sectional energy-dispersive-X-ray (EDX) spectroscopy elemental mapping, by using scanning electron microscopy (SEM) of copper nitride thin films, grown by RF-magnetron sputtering, on transparent glass substrates, at room temperature. We have previously performed the FIB sample preparation, before making the EDX measurements.

4. WVASE®-model ellipsometric fitting

In order to determine the optical constants, n and k, of the Cu_3N thin films, a commercial software package (WVASE32 version 3.774, J.A.Woollam), is used to construct a suitable model in order to fit the ellipsometric data ψ and Δ, respectively. It is certainly well-known that an *ideal* thin film must be homogeneous and have a perfect flat surface, and that very infrequently happens in reality. The most-usually found cases are obviously *non-ideal* thin films, with a surface roughness at top, thickness non-uniformity, and a optical-constant variation from the top, down to the bottom, through the whole thin-film thickness [23].

The two ellipsometric parameters ψ and Δ, respectively, are related to the ratio of the Fresnel reflection coefficients, R_p and R_s, for p- and s-polarized light, respectively, as expressed in Eq.(1):

$$\rho \equiv \frac{R_p}{R_s} = \tan(\psi) e^{i\Delta}. \quad (1)$$

The ratio, ρ, of the two values is measured by the VASE technique, and, as consequence, the obtained values are very accurate and reproducible [23]. For the present thin-film sample under study (a Cu_3N thin film onto a thick-transparent-glass substrate), the Sellmeier dispersion function is employed in order to describe the optical properties of the transparent glass substrate. In the optical model for the Cu_3N thin film, such a film is divided into two equivalent parts.

Preprints (www.preprints.org) | NOT PEER-REVIEWED | Posted: 19 May 2023 doi:10.20944/preprints202305.1426.v1

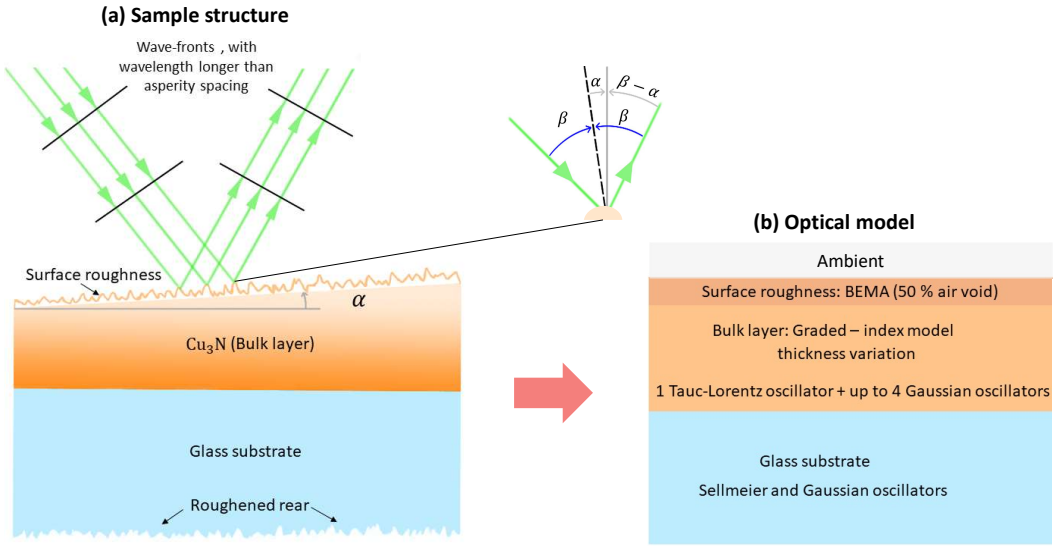

Figure 5. (a) Schematic diagram of the sample structure under study, consisting of a copper nitride thin film onto a transparent glass substrate, with the rear surface roughened. (b) Adopted model for the fitting carried out in the present ellipsometric analysis.

One of them is a *bulk* planar Cu_3N layer, and its corresponding bulk thickness is denoted by d_{bulk}. The other one is a surface-roughness layer consisting of a mixture of air void and Cu_3N material; the thickness of the vertical surface roughness is denoted by d_{rough}. To clearly illustrate the proposed model, a schematic sketch of this model is shown in Fig. 5. For the surface-roughness layer, a Bruggeman-effective-medium approximation is commonly appropriate, whereby the medium consists of the mixture of x % of air void and $(x-1)$ % Cu_3N material, and where it is verified that $0 < x < 100$. For the Cu_3N layer (with thickness d_{bulk}), the Tauc-Lorentz (TL) and Gaussian (Gau) oscillators were successfully adopted to accurately described the complex dielectric function of the Cu_3N material [22,28]. The 'TL' and 'Gau' oscillator functions are given by Eqs. (2)-(5), respectively [23]:

$$\varepsilon_{n\_\text{T-L}} = \varepsilon_{n1} + i\varepsilon_{n2}, \tag{2}$$

where

$$\varepsilon_{n2} = \begin{cases} \dfrac{A_n E_{on} C_n (E - E_{gn})^2}{(E^2 - E_{on}^2)^2 + C_n^2 E^2} \cdot \dfrac{1}{E}, & \text{if} \quad E > E_{gn} \\ 0 \qquad\qquad\qquad\qquad\quad , & \text{if} \quad E \leq E_{gn} \end{cases} \tag{3}$$

and

$$\varepsilon_{n1} = \frac{2}{\pi} \mathscr{P} \int_{E_{gn}}^{\infty} \frac{\xi \varepsilon_{n2}(\xi)}{\xi^2 - E^2} d\xi. \tag{4}$$

In Eqs. (2) and (3), the subscript 'T-L' encompasses the fact that this particular dispersion model is based upon the Tauc joint density of states, and the Lorentz oscillator. The four fitting parameters are: A_n, E_{on}, C_n and E_{gn}, respectively, and where these parameters are all of them expressed in eV. Here, $\mathscr{P}$ stands for the Cauchy principal value of the two previous integrals.

The 'Gau' oscillator function, on the other hand, is given by the following expression:

$$\varepsilon_{n\_\text{Gau}} = \varepsilon_{n1} + i\varepsilon_{n2}, \tag{5}$$

where

$$\varepsilon_{n2} = A_n e^{((E-E_n)/\sigma)^2} - A_n e^{-((E+E_n)/\sigma)^2}, \tag{6}$$

Preprints (www.preprints.org) | NOT PEER-REVIEWED | Posted: 19 May 2023 doi:10.20944/preprints202305.1426.v1

and

$$\sigma = \frac{Br_n}{2\sqrt{\ln(2)}}, \tag{7}$$

and, finally,

$$\varepsilon_{n1} = \frac{2}{\pi}\mathscr{P}\int_0^{\infty} \frac{\xi\varepsilon_{n2}(\xi)}{\xi^2 - E^2} d\xi. \tag{8}$$

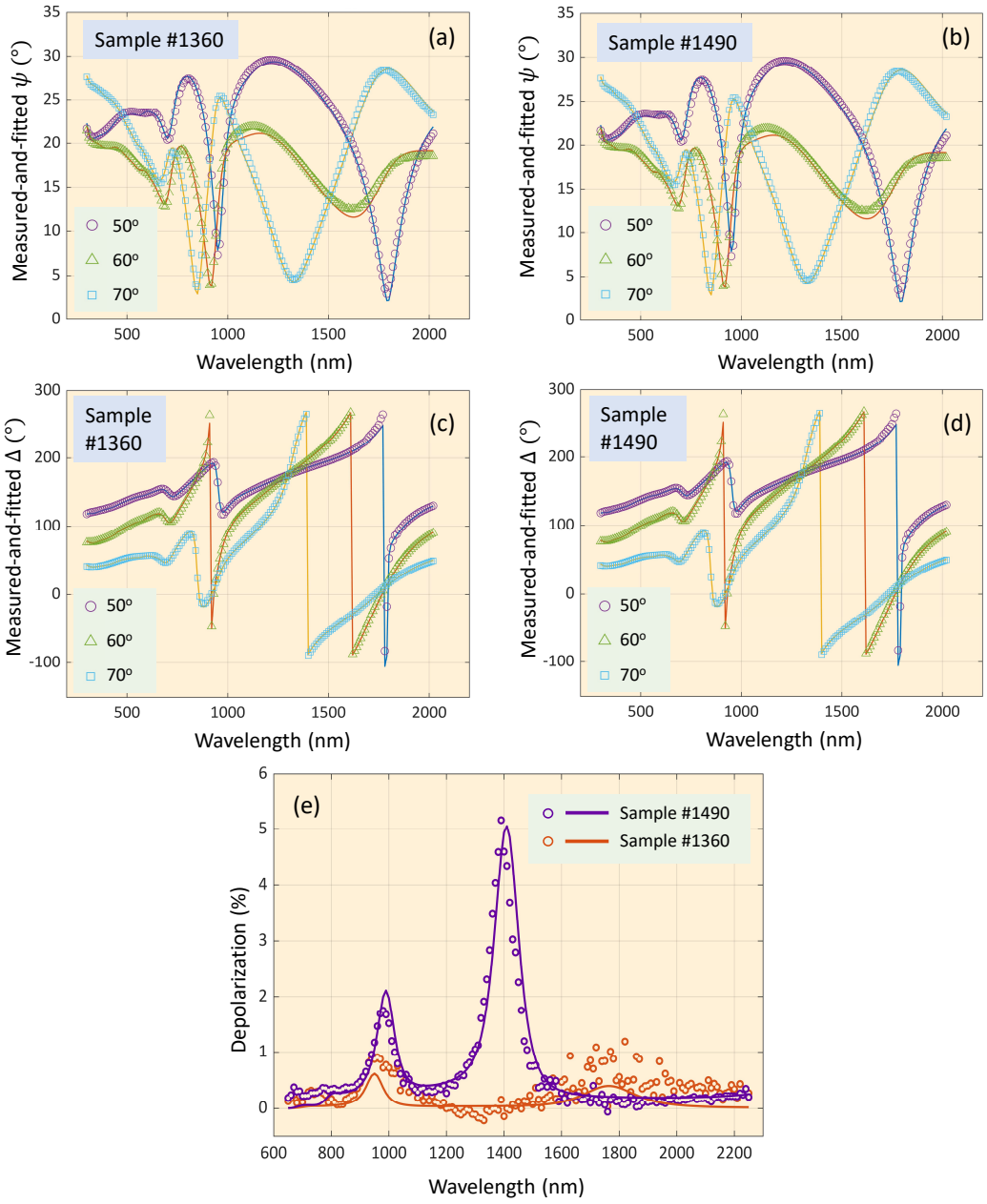

Figure 6. (a) and (b) the measured-and-fitted ψ-values at the three angles of incidence of 50°, 60°, and 70°, in the wavelength range from 300 nm up to 2200 nm. (c) and (d), the measured-and-fitted Δ-values at the same previous angles and in the same previous experimental spectral range.(e) Depolarization spectra of the two representative copper nitride thin films at the angle of incidence of 60°. The curve fitted by employing the ellipsometric method described in-depth in the text; is also presented with a solid line. The depolarization has been modeled with 2.3 % and 5.2 % thickness nonuniformity in the cases of sample #1360 and #1490, respectively.

Preprints (www.preprints.org) | NOT PEER-REVIEWED | Posted: 19 May 2023 doi:10.20944/preprints202305.1426.v1

The three fitting parameters that are employed for the WVASE® fitting in this particular case are A_n, where the corresponding unit is dimensionless, E_n, where the unit is eV, and Br_n, where the unit is also eV.

Another ellipsometric model which will be employed in this analysis is the aforementioned BEMA model. This model makes the *self-consistent* choice of the *host-material* complex dielectric function equals to the final *effective* complex dielectric function of the multi-constituent material. The BEMA model requires the numerical solution of the following equation, for two constituents A and B, respectively:

$$f_{\mathrm{A}}\frac{\tilde{\varepsilon}_{\mathrm{A}}-\tilde{\varepsilon}}{\tilde{\varepsilon}_{\mathrm{A}}+2\tilde{\varepsilon}}+f_{\mathrm{B}}\frac{\tilde{\varepsilon}_{\mathrm{B}}-\tilde{\varepsilon}}{\tilde{\varepsilon}_{\mathrm{B}}+2\tilde{\varepsilon}}=0. \tag{9}$$

For the glass substrate the expression for the dielectric function is as follows:

$$\varepsilon_{n\_\mathrm{pole}}=\frac{\mathrm{A}_n}{E_n^2-E^2}. \tag{10}$$

It is the so-called Pole or Sellmeir term, which corresponds to a Lorentz oscillator with zero broadening. Some *gaussian* oscillators will also be added in order to complete the accurate description of the Corning® transparent glass substrate used.

It is worth pointing out that several studies have reported that the variation of the two optical constants, n and k, respectively, of a thin film along the normal direction to the film, is most frequently owing to the drifting of the deposition-process parameters [27]. This fact suggest that the optical model with an one-dimensional graded index, along the normal direction to the thin layer, can reasonably be adopted in the present case. *Graded* layers work by introducing a series of homogeneous layers, whose optical constants slightly-and-gradually change in each of the successive layers.

Figure 5a displays a very detailed and realistic schematic of a Cu_3N thin film onto a bare transparent glass substrate. Figure 5b, on the other hand, is the suggested model to accurately fit the measured ψ and Δ parameters, where a BEMA model with 50-%-of-air-void is employed in order to give an account for the effect of the existing Cu_3N rough surface; a one-dimensional graded-index model throughout the whole film, from the bottom to the top, combined with one T-L oscillator and up to four Gau oscillators are employed in order to fully describe the three Cu_3N-bulk-flat layers under study. Furthermore, two zero-width oscillators, and two additional Gau oscillators are adopted in order to accurately describe the Corning®-glass transparent substrate employed in our RF-magnetron-sputtering depositions.

Next, we must first define some convenient statistical quantity, which is called a *maximum likelihood* estimator. We will elaborate now a little bit more about that aspect by stating that the principle of maximum likelihood assumes that the population sample is a fair representation of the whole population, and selects a correct estimator that maximizes the probability density function (in continuous cases), or the probability mass function (in discrete cases). This particular choice represents the level of accuracy in correctly matching the data obtained from the *constructed* optical model, to our experimentally-measured data [29]. It has to be mentioned that the parameters of the particular oscillators were all appropriately varied in the process. This maximum-likelihood estimator must be necessarily positive, and go down to zero (or, at least, go down to an *absolute* minimum), when the model-generated data *exactly* matches the experimentally-measured data. The present Woollam WVASE32 software employs the following mean-square error (MSE) estimator:

$$\mathrm{MSE}=\sqrt{\frac{1}{2N-M}\sum_{i=1}^{N}\left[\left(\frac{\psi_i^{\mathrm{mod}}-\psi_i^{\mathrm{exp}}}{\sigma_{\psi,i}^{\mathrm{exp}}}\right)^2+\left(\frac{\Delta_i^{\mathrm{mod}}-\Delta_i^{\mathrm{exp}}}{\sigma_{\Delta,i}^{\mathrm{exp}}}\right)^2\right]}=\sqrt{\frac{1}{2N-M}\chi^2}, \tag{11}$$

Preprints (www.preprints.org) | NOT PEER-REVIEWED | Posted: 19 May 2023 doi:10.20944/preprints202305.1426.v1

where N is the number of (ψ, Δ) ellipsometric-angle pairs, M is the total number of *free* fitting parameters in the adopted optical model, and the introduced values of σ are the corresponding standard deviations associated to all the collected, measured data points. Another very common estimator, the so-called *chi-square*, χ^2, is introduced in Eq.11, for the sake of illustration.

Table 3. Deposition conditions of the Cu_3N layers. The values of best-fit parameters obtained by employing the VASE ellipsometer (J.A.Woollam Co.), and their corresponding experimental uncertainties.

Sample #1360					
Cu_3N-Visible-and-UV-oscillator-coefficients					
Oscillator	Type	A, amplitude	E_0, eV	C, eV	E_g, eV
1	Tauc-Lorentz	0.707 ± 0.4	1.12 ± 0.01	0.367 ± 0.03	0.751 ± 0.01
Oscillator	Type	A, amplitude	E_0, eV	Br, eV	
2	Gaussian	5.19 ± 0.1	3.94 ± 0.03	1.43 ± 0.1	
3	Gaussian	4.64 ± 0.02	2.62 ± 0.02	1.00 ± 0.05	
4	Gaussian	0.50 ± 0.09	1.80 ± 0.01	0.57 ± 0.09	
MSE: 4.007					
d_{rough}: 41.6 ± 0.2 nm					
d_{bulk}: 388.4 ± 0.4 nm					
Thickness variation: 2.3 ± 0.3 %					
Index variation: -13.2 ± 0.02 %					
Offset, $\varepsilon_{1\infty}$: 2.82 ± 0.05					
E_u: 96 meV					
Sample #1490					
Cu_3N-Visible-and-UV-oscillator-coefficients					
Oscillator	Type	A, amplitude	E_0, eV	C, eV	E_g, eV
1	Tauc-Lorentz	9.33 ± 0.4	2.46 ± 0.01	0.765 ± 0.03	0.872 ± 0.02
Oscillator	Type	A, amplitude	E_0, eV	Br, eV	
2	Gaussian	4.69 ± 0.1	3.96 ± 0.06	2.79 ± 0.06	
MSE: 6.686					
d_{rough}: 46.1 ± 0.2 nm					
d_{bulk}: 563.7 ± 0.7 nm					
Thickness variation: 5.2 ± 0.1 %					
Index variation: -14.1 ± 0.02 %					
Offset, $\varepsilon_{1\infty}$: 2.39 ± 0.06					
E_u: 242 meV					
Sample #1460					
Cu_3N-Visible-and-UV-oscillator-coefficients					
Oscillator	Type	A, amplitude	E_0, eV	C, eV	E_g, eV
1	Tauc-Lorentz	35.0 ± 4.3	2.50 ± 0.029	1.29 ± 1.16	1.56 ± 0.01
Oscillator	Type	A, amplitude	E_0, eV	Br, eV	
2	Gaussian	1.82 ± 1.0	4.25 ± 0.11	0.540 ± 0.41	
3	Gaussian	1.33 ± 0.91	4.19 ± 0.83	2.53 ± 0.60	
4	Gaussian	0.153 ± 0.07	1.94 ± 0.036	0.196 ± 0.08	
MSE: 9.738					
d_{rough}: 22.1 ± 0.3 nm					
d_{bulk}: 310.4 ± 0.5 nm					
Thickness variation: ≈ 0 %					
Index variation: -4.81 ± 0.2 %					
Offset, $\varepsilon_{1\infty}$: 2.82 ± 0.05					
E_u: 176 meV					

f

The measured and simulated values of ψ and Δ, at the three selected angles of incidence of 50°, 60°, and 70°, respectively, in the UV/Visible/NIR wavelength range from 300 up to 2200 nm, are depicted in Fig. 6a-d. It can clearly be noticed that excellent fitting results are obtained for both

 doi:10.20944/preprints202305.1426.v1

ellipsometric parameters, ψ and Δ, respectively. By the optimization process carried out, it is found that the best fitting results are achieved with: (*i*) a graded-index variation from bottom to top of aproximately 5.0 to 14.0 %, and (*ii*) thicknesses of the Cu_3N bulk layer and surface-roughness layer, d_{bulk} and d_{rough}, of around 310 to 570 nm and close to 20 to 50 nm, respectively, all of them in close agreement with those estimated values from the independent SEM and AFM measurements (see Figs. 2 and 3). Lastly, the calculated parameters belonging to the best fit for each Cu_3N sample, and those experimentally-measured values, are all of them listed in Table 3. It has also been found that, if either the adopted graded-index model was *not* included, or all the oscillators are fully-chosen T-L oscillator, the associated fitting results are notably worsened, causing an incorrect derivation of the optical constants. Contrarily, if all the oscillators are adopted Gau oscillators, the resulting optical constants are just slightly affected.

It is next shown that a measurable *depolarization* effect has clearly been observed in all the specimens. To begin with, it must be said that depolarization does occur if the reflected beam contains multiple polarization states. In the case of *isotropic* samples —as we assume in our case of the copper-nitride thin films— depolarization, D, can be calculated from the values of the two ellipsometric angles, ψ and Δ, respectively, as follows:

$$D = 1 - [(\cos 2\psi)^2 + (\sin 2\psi \cos \Delta)^2 + (\sin 2\psi \sin \Delta)^2]. \tag{12}$$

Depolarization spectra of the Cu_3N samples were measured by also employing the Woollam VASE ellipsometer, in the spectral range of 300-2200 nm; some of these spectra are shown in Fig. 6e. Evaluation of the depolarization spectra was also performed with the WVASE32 software.

5. Results and discussion

5.1. Complex index of refraction and dielectric function

By using the previous best-fitting results, we can find the corresponding *dispersive* n-and-k values. They are displayed in Fig. 7, and it has to be emphasized that we extend our values of the complex refractive index, $\tilde{n} = n - ik$, up to the NIR wavelength of 2500 nm; it represents an excellent opportunity in order to perform the useful design and simulations on high-efficiency solar cells. To additionally confirm the correctness of ellipsometrically-calculated optical constants, the independent comparison of the measured-and-predicted values of the normal-incidence transmission, in the wavelength range under study, is shown in Fig. 7. We have not used in our study the *multi-sample* approach; instead, we have *calculated* the normal-incidence transmission based exclusively on the results found from the ellipsometric analysis. For this purpose, we have carefully tried to carry out all the measurements on the very same spot of each thin-film sample. The difference observed between the predicted and the experimental values of transmittance are mainly due to the unavoidable differences in the positions on the sample, and also to the experimental uncertainty of the transmission-intensity measurements performed by the Woollam single-beam VASE ellipsometer. However, it can be observed that an excellent agreement between the experimentally-measured and calculated transmission spectra is reached in our samples; thus, it gives an extra confidence upon n and k exclusively determined from the VASE measurements, in the spectral range from 300 up 2200 nm. Moreover, it is worth pointing out that the color of our semi-transparent Cu_3N thin films is reddish dark-brown, or mahogany red (see the respective insets in Fig. 8 showing the visual appearance of the three samples). The differences in color of the investigated Cu_3N samples are obviously a direct consequence of their measured transmission spectra, as shown in Fig. 8.

Let's now discuss the *optical dispersion*, or chromatic dispersion, which is an important parameter in order to more deeply understand the optical properties of quasi-transparent (weakly-absorbing) Cu_3N films. Optical dispersion is the required parameter in order quantify the change of the material's refractive index with respect to the incident-light wavelength, $dn/d\lambda$. Usually, in non-absorbing materials the real refractive index increases with incident-light frequency, that is, $dn/d\lambda < 0$, in the *normal* dispersion regimen. In the opposite case, where $dn/d\lambda > 0$, we are

Preprints (www.preprints.org) | NOT PEER-REVIEWED | Posted: 19 May 2023 doi:10.20944/preprints202305.1426.v1

in the *anomalous-dispersion* regimen, that is, increasing the light frequency results in a decrease in the real index of refraction. In our RF-sputtered Cu_3N samples, the values of vacuum-light wavelength where the transition takes place (the so-called refractive-index-threshold wavelength), *i.e.*, where $dn/d\lambda = 0$, are 530 nm and 560 nm, for the two representative samples, #1360 and #1490, respectively (see Figs. 7a and 7b).

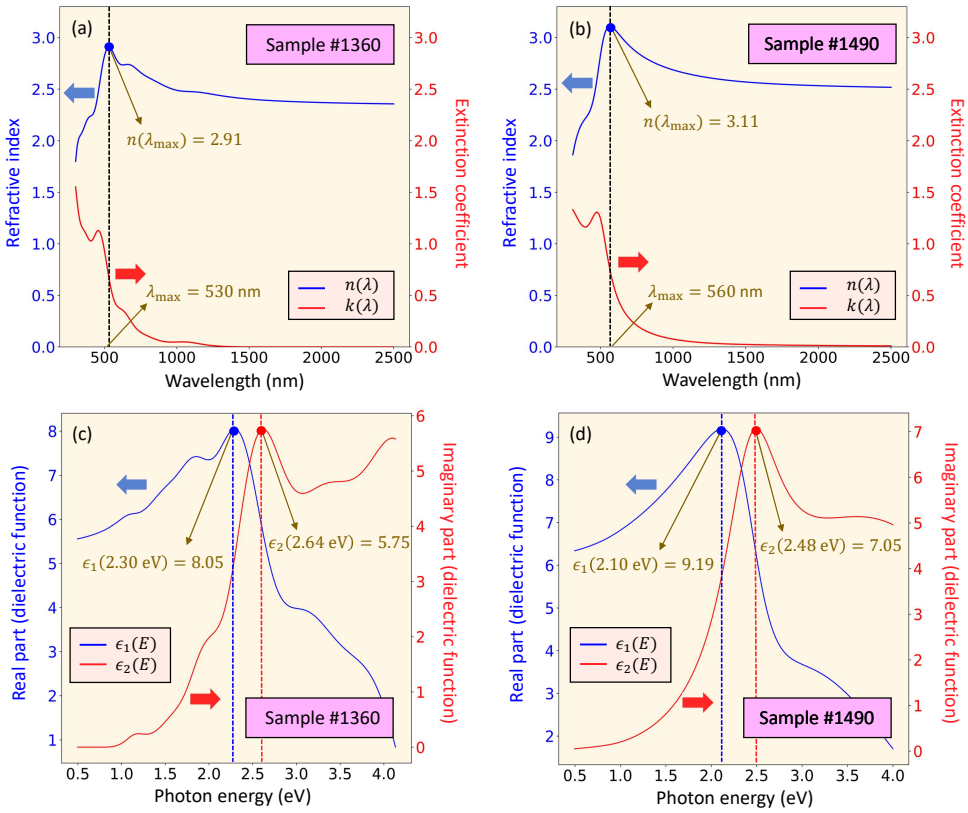

Figure 7. (a) Real part of the complex refractive index, n, and (b) imaginary part of the complex refractive index, k, of the Cu_3N thin layers. (b) The real, ε_1, and imaginary, ε_2, parts of the complex dielectric function.

The real and imaginary parts of the complex dielectric function, ε_1 and ε_2, respectively, on the other hand, are obtained as a function of the refractive index, n, and extinction coefficient, k, from the fundamental expressions (based upon the basic relationship, $\tilde{\varepsilon} = \tilde{n}^2$):

$$\begin{aligned} \varepsilon_1 &= n^2 - k^2, \\ \varepsilon_2 &= 2nk. \end{aligned} \tag{13}$$

Concerning the obtained shape of the real and imaginary parts of the complex dielectric function upon photon energy (see Figs. 7c and 7d), typical for a semiconductor or insulator material, it agrees certainly well with previously reported data [4]. However, in our particular Cu_3N specimens, the magnitude of the peaks of ε_1 and ε_2, about 8.0 and 6.0, respectively, is a multiplying factor of around 1.5 and 2.0, respectively, smaller than those other values reported in [4] (all of them, one order of magnitude thinner than our Cu_3N films, and with an optical gap of 1.65 eV). These results could be an effect strongly correlated with the values of the film thickness, which is very much thicker in our presently-prepared Cu_3N layers.

Preprints (www.preprints.org) | NOT PEER-REVIEWED | Posted: 19 May 2023 doi:10.20944/preprints202305.1426.v1

5.2. Additional calculation of the indirect-and-direct Tauc gap and Urbach energy.

At this point of the paper, it must be stressed that each semiconductor material has *both* direct and indirect gaps; whichever is lower shall determine the specific nature of its energy-band gap. It has to be borne in mind that the band gap is a property basically associated to the *lattice constant* of the material; in fact, its band gap can readily be changed by varying the value of its lattice constant. This particular value can be changed by various ways, *e.g.*, by applying pressure, by heating or cooling, or by mixing with another semiconductor material. Both, the direct and indirect band gaps, will be modified with the change of the lattice constant, but at different rates.

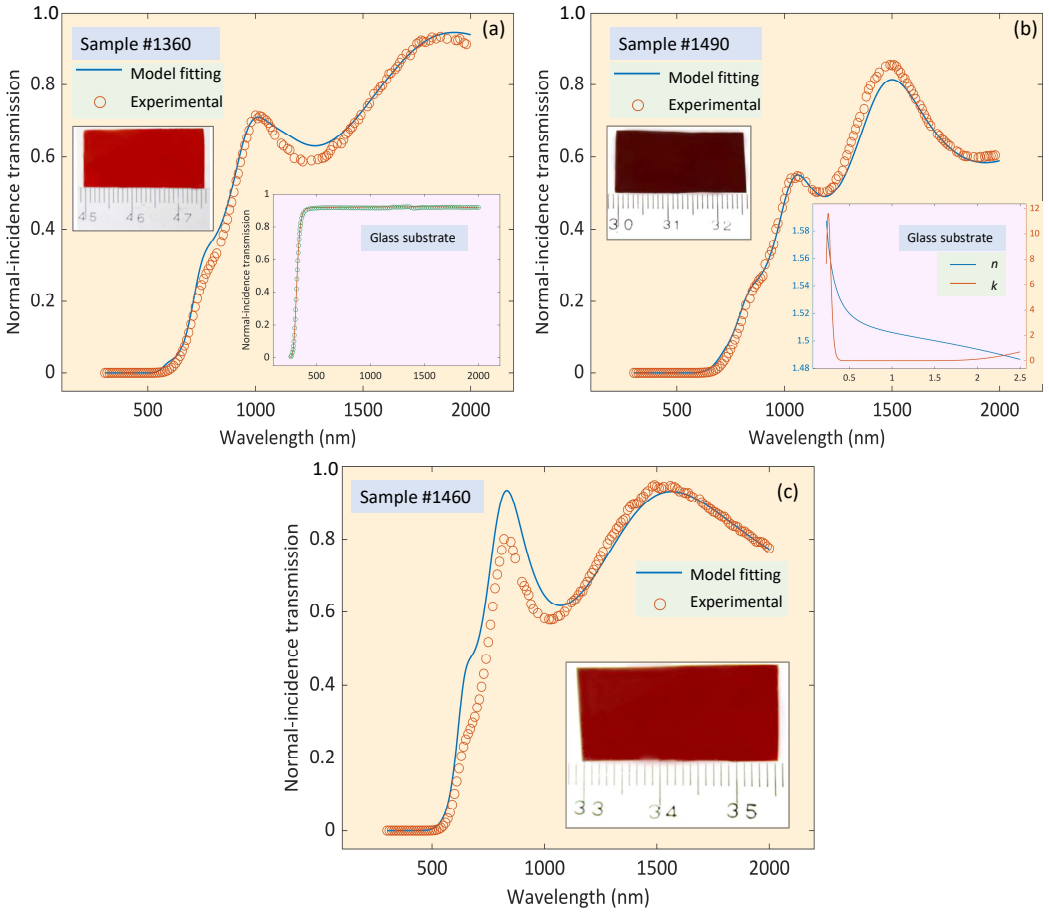

Figure 8. Experimentally-measured optical-transmission intensity data, acquired by using the varied-angle spectroscopic ellipsometer, and the computationally-predicted values of transmittance in the studied spectral range: (a) sample #1360, (b) sample #1490, and (c) sample #1460.

Regarding the calculation of the energy-band gap of the investigated Cu_3N thin-layer material, it should be recalled that while investigating the electronic properties of *a*-Ge, Tauc *et al.* [30] proposed a nowadays, well-established method for determining the band gap by using optical data, plotted conveniently versus photon energy. The optical-absorption strength depends upon the difference between the photon energy and the band gap, and it is expressed by the following relation:

$$(\alpha\hbar\omega)^{1/m} = A(\hbar\omega - E_g), \tag{14}$$

where $\hbar$ is the Dirac's constant, α $(= 4\pi k/\lambda)$ is the absorption coefficient, E_g is the band gap, and A is a proportionality constant (energy-independent), also called the band-tailing parameter; A it is actually a function of the refractive index of the material and its carrier effective mass. The value of the exponent denotes the actual nature of the corresponding electronic transition, whether *allowed* or

Preprints (www.preprints.org) | NOT PEER-REVIEWED | Posted: 19 May 2023 doi:10.20944/preprints202305.1426.v1

forbidden, and whether *direct* or *indirect*:

(*i*) direct and allowed transitions, $m = 1/2$,
(*ii*) direct and forbidden transitions, $m = 3/2$,
(*iii*) indirect and allowed transitions, $m = 2$,
(*iv*) indirect and forbidden transitions, $m = 3$.

Usually, the allowed transitions clearly dominates the basic optical-absorption processes, giving either $m = 1/2$ or $m = 2$, for direct and indirect electronic transitions, respectively. Hence, the main procedure for a 'Tauc analysis' is to accurately determine optical-absorption-coefficient data that spans a photon-energy range from below the band-gap transition to above it. Thus, plotting $(\alpha\hbar\omega)^{1/m}$ against $\hbar\omega$ is a way of testing either $m = 1/2$ or $m = 2$, in order to compare which provides the better fit, and thus identifies the correct electronic-transition type. We will next experimentally find that the smaller value of the indirect band gap is, as expected, accompanied with the larger spectral range of agreement in the fit, in its corresponding 'Tauc-extrapolation plot'. It has to be emphasized that the calculated value of the *indirect* band gap for our Cu_3N layers, is well within the *optimal* band-gap range for solar-cell applications, which is approximately 1.4-1.5 eV.

The indirect band gap was calculated by plotting $(\alpha\hbar\omega)^{1/2}$ versus $\hbar\omega$ curve, and by extrapolating the full line to the abscissa of $\hbar\omega$ (see Fig. 9). Similarly, the direct band gap was calculated by extrapolating the full line to the abscissa of $\hbar\omega$, in the $(\alpha\hbar\omega)^2$ versus $\hbar\omega$ curve (see again Fig. 9). The direct and indirect band-gap values for the two representative Cu_3N specimens #1360 and #1490 are found to be 1.45 and 1.46 eV, respectively, and 2.21 and 2.14 eV, respectively. It must now be mentioned that there is generally highly inconsistent-and-discrepant information about the optical properties of Cu_3N films; those optical properties of Cu_3N have been the subject of strong controversy with regard to the bulk band-gap values, as well as the precise nature of its electronic transitions. The band-gap values are found to widely vary between 0.23 eV and 2.38 eV, and the concrete nature of the band-gap transition has paradoxically been reported to be *both* direct as well as indirect.

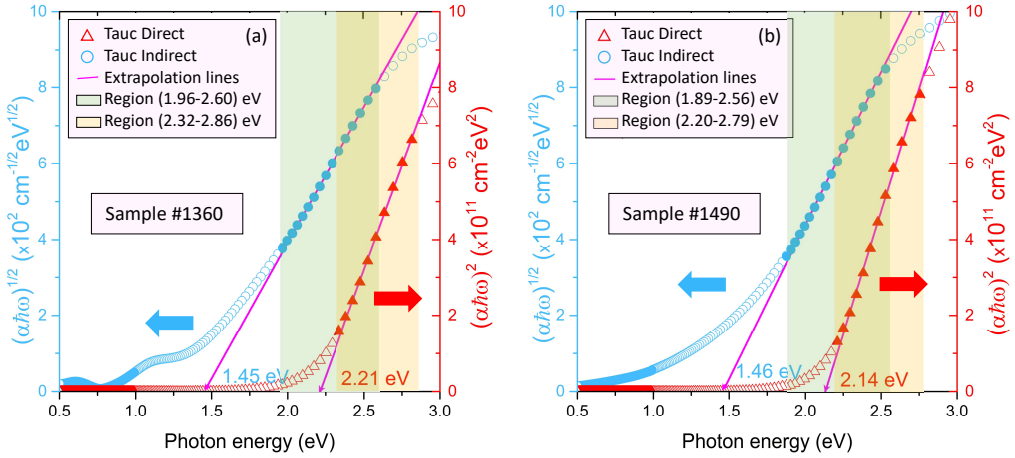

Figure 9. $(\alpha\hbar\omega)^{1/2}$ versus $\hbar\omega$ plot for the determination of the *indirect* energy-band gap, and $(\alpha\hbar\omega)^2$ versus $\hbar\omega$ plot for the calculation of the *direct* energy-band gap, for the samples (a) #1360, and (b) #1490, respectively.

Going even more deeply into the optical properties of the Cu_3N thin films, it is well known that the structural disorder in a material gives rise to a tailing of the density of states in the forbidden energy gap, known as Urbach tail, and the width of the tail is the Urbach energy, E_u. In such a way that higher value of E_u means lower degree of structural order. The absorption coefficient, α, is linked to the structural-order parameter, E_u, by the following expression [31–35]:

Preprints (www.preprints.org) | NOT PEER-REVIEWED | Posted: 19 May 2023 doi:10.20944/preprints202305.1426.v1

$$\alpha = \alpha_0 \exp\left(\frac{\hbar\omega}{E_u}\right), \tag{15}$$

where α_0 is a constant, and the structural parameter, E_u, is, therefore, obtained from the linear fitting of the semilogarithmic graph of α versus $\hbar\omega$ (see Fig. 10, where the *optical-absorption edge* is shown). Specifically, the inverse of the slope gives the value of the parameter E_u: The value is found to be 96 meV in the particular case of the specimen #1360, 242 meV in the case of the specimen #1490, and 170 meV for the specimen #1460 (see Table 3, and also Fig. 10). From these values of E_u, it is inferred that in the first of the three Cu_3N samples, with a different gaseous environment of $N_2 + Ar$, the degree of *structural disorder* is notably smaller than in the other two samples, with a gaseous environment of just N_2.

Moreover, these previous values of E_u are indeed comparable to those reported by other authors in the case of Cu_3N thin films, interpreting this Urbach energy as the bandwidth of the electronic states located within the band-gap width. That is, the Urbach tail is associated to the density of *localized* electronic states. In other words, the calculated value of E_u is an excellent indicator of the level of structural *defects* existing in the atomic structure of the semiconductor material under study.

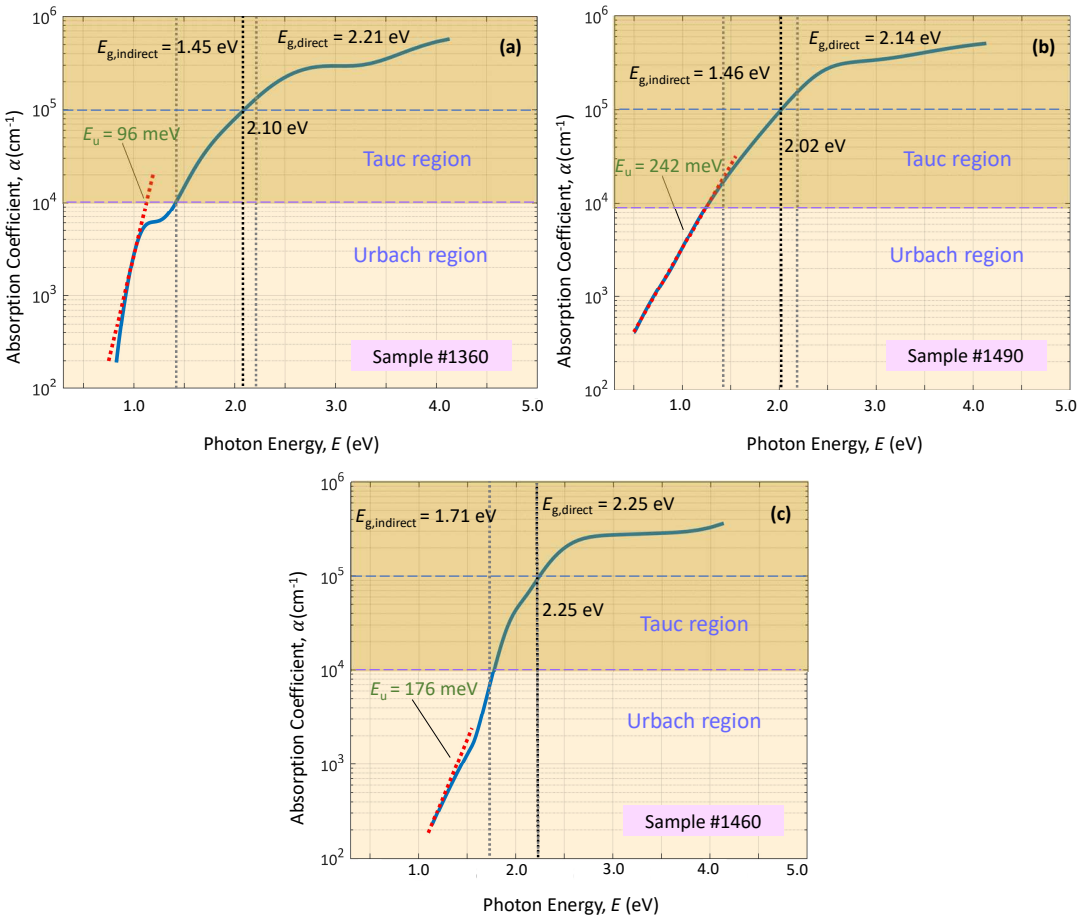

Figure 10. A semilogarithmic plot of the absorption coefficient as a function of incident photon energy for copper nitride thin films grown on glass substrates. The exponential dependence is valid in the near band-edge region. The slope of the linear fit is used to calculate the Urbach-energy parameter, E_u.

Concerning the electronic properties of our material under investigation, it ought to be indicated that the calculated energy-band structure of Cu_3N shows that it is undoubtedly a semiconductor, at ambient pressure [25]. Cu orbitals mainly form the conduction bands especially at the R and M

 doi:10.20944/preprints202305.1426.v1

points of the *first Brillouin zone* (see all the details shown in the inset of Fig. 1c), and the valence band consist of $2p$ orbital of N atoms for the same symmetric points. From partial density of states, strong hybridization has been seen between the N and Cu states, mostly related to both N $2p$ and Cu $3d$ orbitals, respectively. The maximum valence band is at the R point of the first Brillouin zone, and the minimum conduction band is at the M point. It was finally concluded that taking into account all possible direct and indirect electronic transitions, the first possible transition is that between the highest occupied state at the R point, and the lowest occupied state at the M point. This unambiguously shows that Cu_3N is an *indirect-band-gap* semiconductor material, as it has clearly been corroborated in our work.

6. Conclusions

(*i*) In the present investigation, polycrystalline Cu_3N thin films were deposited by making use of RF-magnetron sputtering, at room-temperature, a total pressure of 5.0 Pa, and by using *two* different gaseous environments of N_2 and $N_2 + Ar$, respectively. The XRD patterns showed that the Cu_3N thin films exhibited an *anti*-ReO_3 structure. In order to enrich the depth of the analysis of the semiconductor material, AFM, SEM (by using FIB sample preparation), and EDX measurements, were systematically performed in all the RF-sputtered thin layers.

(*ii*) The complex refractive index of the RF-sputtered Cu_3N thin films was accurately determined via VASE measurements, at three angles of incidence, 50°, 60°, and 70°, respectively. The constructed ellipsometric model consisted of a one-dimensional graded-index plus a BEMA model with 50 %-air-void, in order to describe both, the bulk Cu_3N layer and the rough surface. The experimentally-measured, normal-incidence transmission spectrum, and the predicted transmission spectrum based upon the obtained ellipsometric results, show a reasonably good agreement in all the cases. The calculated optical constants allow to be able to design and simulate a potential photovoltaic electronic device. The absorption strength, on the other hand, reaches a magnitude of 1.0×10^5 cm^{-1} from approximately 2.0 eV, suggesting a very promising potential for solar-cell applications. The lower Urbach energy value, for the case of the sample #1360 with a gaseous environment of $N_2 + Ar$, is associated with the presence of much lower level of defects in its atomic structure, in comparison with the samples of a gaseous environment of just N_2.

(*iii*) Last but not the least, the investigated Cu_3N material with the corresponding values of E_g can unambiguously be considered satisfactory for use as a solar-light absorber material. The specific aspect of the solar-cell technology that could certainly benefit the most from the use of the Cu_3N thin-film material would be that related to the photovoltaic electronic devices, as they provide a flexible texture, and are relatively *inexpensive* in order to be manufactured.

Acknowledgments

This research was funded by MCIN/AEI/10.13039/501100011033, grant number PID2019-109215RB-C42. M.A. Rodríguez-Tapiador also acknowledges partial funding through MEDIDA C17.I2G: CIEMAT. Nuevas tecnologías renovables híbridas, Ministerio de Ciencia e Innovación, Componente 17 “Reforma Institucional y Fortalecimiento de las Capacidades del Sistema Nacional de Ciencia e Innovación”. Medidas del plan de inversiones y reformas para la recuperación económica funded by the European Union—NextGenerationEU.

References

1. Figuera, C.A.; Del Rosario, G.; Pugliese, D.; Rodríguez-Tapiador, M.I.; Fernández, S. Effect of Argon on the Properties of Copper Nitride Fabricated by Magnetron Sputtering for the Next Generation of Solar Absorbers. *Materials* **2022**, *15*, 8973.
2. Rodríguez-Tapiador, M.I.; Merino, J.; Jawhari, T.; Muñoz-Rosas, A.L.; Bertomeu, J.; Fernández, S. Impact of the RF Power on the Copper Nitride Films Deposited in a Pure Nitrogen Environment for Applications as Eco-Friendly Solar Absorber. *Materials* **2023**, *16*, 1508.
3. Zakutayev, A. Design of nitride semiconductors for solar energy conversion. *J. Mater. Chem. A* **2016**, *4*, 6742.
4. Borsa, D.M.; Boerma, D.O. Growth, structural and optical properties of Cu_3N films. *Surface Science* **2004**, *148*, 95.
5. Jiang, A.; Qi, M.; Xiao, J. Preparation, structure, properties, and application of copper nitride (Cu3N) thin films: A review. *Journal of Materials Science Technology* **2018**, *34*, 1467–1473.

6. Bouazza, A. Deposition of Thin Films Materials used in Modern Photovoltaic Cells. *International Journal of Thin Film Science and Technology* **2022**, *11*, 313.
7. Paredes, P.; Rauwel, E.; Rauwel, P. Surveying the Synthesis, Optical Properties and Photocatalytic Activity of Cu3N Nanomaterials. *Nanomaterials* **2022**, *12*, 2218.
8. Tilemachou, A.; Zervos, M.Z.; Othonos, A.; Pavloudis, T.; Kioseoglou, J. p-Type Iodine-Doping of Cu_3N and Its Conversion to γ-CuI for the Fabrication of γ-CuI/Cu_3N p-n Heterojunctions. *Electronic Materials* **2022**, *3*, 15.
9. Hahn, U.; Weber, W. Electronic structure and chemical-bonding mechanism of Cu_3N, Cui_3NPd, and related Cu(I) compounds. *Physical Review B* **1996**, *53*, 12684.
10. Ghoohestani, M.; Karimipour, M.; Javdani, Z. The effect of pressure on the physical properties of Cu3N. *Physica Scripta* **2014**, *89*, 035801.
11. Sahoo, G.; Meher, S.R.; Mahaveer, K.J. Room temperature growth of high crystalline quality Cu_3N thin films by modified activated reactive evaporation. *Materials Science and Engineering: B* **2015**, *191*, 7.
12. Matsuzaki, K.; Okazaki, T.; Lee, Y.S.; Hosono, H.; Susaki, T. Controlled bipolar doping in Cu_3N (100) thin films. *Applied Physics Letters* **2014**, *105*.
13. Márquez, E.; Blanco, E.; García-Vázquez, C.; Díaz, J.M.; Saugar, E. Spectroscopic ellipsometry study of non-hydrogenated fully amorphous silicon films deposited by room-temperature radio-frequency magnetron sputtering on glass: Influence of the argon pressure. *Journal of Non-Crystalline Solids* **2020**, *547*, 120305.
14. Márquez, E.; Díaz, J.; García-Vázquez, C.; Blanco, E.; Ruíz-Pérez, J.; Minkov, D.; Angelov, G.; Gavrilov, G. Optical characterization of amine-solution-processed amorphous AsS2 chalcogenide thin films by the use of transmission spectroscopy. *Journal of Alloys and Compounds* **2017**, *721*, 363.
15. Blanco, E.; Domínguez, M.; González-Leal, J.; Márquez, E.; Outón, J.; Ramírez-del Solar, M. Insights into the annealing process of sol-gel TiO2 films leading to anatase development: The interrelationship between microstructure and optical properties. *Applied Surface Science* **2018**, *439*, 736.
16. Márquez, E.; Ruíz-Pérez, J.; Ballester, M.; Márquez, A.P.; Blanco, E.; Minkov, D.; Fernández, S.M.; Saugar, E. Optical characterization of H-free *a*-Si layers grown by rf-Magnetron sputtering by inverse synthesis using Matlab: Tauc-Lorentz-Urbach Parameterization. *Coatings* **2021**, *11*, 1324.
17. Ballester, M.; García, M.; Márquez, A.P.; Blanco, E.; Minkov, D.; Fernández-Ruano, S.; Willomitzer, F.; Cossairt, O.; Márquez, E. Application of the holomorphic Tauc-Lorentz-Urbach functions to extract the optical constants of amorphous semiconductor thin films. *Coatings* **2022**, *12*, 1549.
18. Marquez, E.; Ballester, M.; Garcia, M.; Cintado, M.; Marquez, A.; Ruiz, J.; Fernández, S.; Blanco, E.; Willomitzer, F.; Katsaggelos, A. Complex dielectric function of H-free a-Si films: Photovoltaic light absorber. *Materials Letters* **2023**, *345*, 134485.
19. Márquez, E.; Saugar, E.; Díaz, J.; García-Vázquez, C.; Fernández-Ruano, S.; Blanco, E.; Ruíz-Pérez, J.; Minkov, D. The influence of Ar pressure on the structure and optical properties of non-hydrogenated a-Si thin films grown by rf magnetron sputtering onto room-temperature glass substrates. *Journal of Non-Crystalline Solids* **2019**, *517*, 32.
20. Wensheng, Y.; Liu, L.; Wangnan, L.; Zhengli, W.; Yue, Z.; Yu, W.; Ke, L.; Meihua, C.; Zhicheng, Z. Toward high efficiency for long-term stable Cesium doped hybrid perovskite solar cells via effective light management strategy. *Journal of Power Sources* **2021**, *510*.
21. Wensheng, Y.; Lingyun, M.; Peiyang, Z.; Mertens, A.; Dottermush, S.; Hang, H.; Zhong, J.; Richrads, B.S. Determination of complex optical constants and photovoltaic device design of all-inorganic $CsPbBr_3$ perovskite thin films. *Optics Express* **2020**, *28*, 15706.
22. Wensheng, Y.; Yi, G.; Deski, B.; Dottermush, S.; Haining, C.; Zhong, J.; Richrads, B.S. Experimental Determination of Complex Optical Constants of Air-Stable Inorganic $CsPbI_3$ Perovskite Thin Films. *Physica Status Solidi* **2020**, *14*, Wiley Online Library.
23. J.A.Woollam Co., I. *Guide to using WVASE spectroscopic ellipsometry data acquisition and analysis software*; J.A.Woollam Co., Inc., 2012.
24. Juza, R.; Hahn, H.; Anorg, Z. Über die Kristallstrukturen von Cu_3N, GaN und InN Metallamide und Metallnitride. *Zeitschrift für anorganische und allgemeine Chemie* **1938**, *239*, 282.
25. Mukhopadhyay, A.K.; Momin, M.A.; Roy, A.; Das, S.C.; Abhijit, M. Optical and Electronic Structural Properties of Cu_3N Thin Films: A First-Principles Study (LDA + U). *ACS Omega* **2020**, *5*, 31918.
26. Ye Sheng, Y.; Inoue, H.; Hultqvist, A.; Hanifi, D.; Salleo, A.; Magyari-Köpe, B.; Nishi, Y.; Bent, S.F.; Clemens, B.M. Copper interstial recombination centers in Cu_3N. *Physical Review B* **2018**, *97*, 245201.
27. Smith, D. *Thin-film deposition: principles and practice*; McGraw-Hill, 1995.
28. Jellison Jr, G.; Modine, F. Parameterization of the optical functions of amorphous materials in the interband region. *Applied Physics Letters* **1996**, *69*, 371.
29. Casella, G.; Berger, R. *Statistical Inference*; Duxbury, Thomson Learning, 2007.
30. Tauc, J.; Grigorovici, R.; Vancu, A. Optical properties and electronic structure of amorphous germanium. *Physica Status Solidi (b)* **1966**, *15*, 627.
31. Urbach, F. The Long-Wavelength Edge of Photographic Sensitivity and of the Electronic Absorption of Solids. *Phys. Rev.* **1953**, *92*, 1324.
32. Tauc, J. *Amorphous and Liquid Semiconductors*; Springer, 1974.
33. Tanaka, K.; Shimakawa, K. *Amorphous Chalcogenide Semiconductors and Related Materials*; Springer, 2011.
34. Cody, G. Urbach edge of crystalline and amorphous silicon: a personal review. *Journal of Non-Crystalline Solids* **1992**, *141*, 3–15.
35. Tanaka, K. Minimal Urbach energy in non-crystalline materials. *Journal of Non-Crystalline Solids* **2014**, *389*, 35.